

# A Baseband Recorder for Radio Pulsar Observations

I. H. Stairs<sup>★</sup>, E. M. Splaver, S. E. Thorsett<sup>†</sup>, D. J. Nice, J. H. Taylor

*Joseph Henry Laboratories and Physics Department, Princeton University, Princeton, NJ 08544 USA*

21 March 2018

## ABSTRACT

Digital signal recorders are becoming widely used in several subfields of centimetre-wavelength radio astronomy. We review the benefits and design considerations of such systems and describe the Princeton Mark IV instrument, an implementation designed for coherent-dedispersion pulsar observations. Features of this instrument include corrections for the distortions caused by coarse quantization of the incoming signal, as well algorithms which effectively excise both narrowband and broadband radio-frequency interference. Observations at 430 MHz using the Mark IV system in parallel with a system using a 250 kHz filter bank and incoherent dedispersion demonstrated timing precision improvement by a factor of 3 or better for typical millisecond pulsars.

**Key words:** instrumentation:detectors – instrumentation:polarimeters – methods: observational – pulsars: general – pulsars: timing

## 1 INTRODUCTION

A fundamental characteristic of radio astronomy is the use of phase-coherent detectors, which coherently amplify the electromagnetic radiation and preserve information about the phases of the wavefronts. An ideal radio telescope backend should take advantage of this phase coherency when recording and detecting data. An effective way to do so is to mix the telescope voltages to baseband, then Nyquist-sample the data stream; however, the resulting

<sup>★</sup> Present address: University of Manchester, Jodrell Bank Observatory, Macclesfield, Cheshire SK11 9DL; is@jb.man.ac.uk

<sup>†</sup> Present address: Department of Astronomy and Astrophysics, University of California, 1156 High St., Santa Cruz, CA 95064 USA

data volumes quickly become very large. Historically, therefore, most wide-bandwidth radio-astronomical observations have been carried out using analogue detection and recording methods, typically a multi-channel spectrometer. An exception is Very Long Baseline Interferometry (VLBI) observations, in which the voltages from different telescopes are recorded to tape, then played back and combined on a custom correlator to determine the visibility function.

In recent years, computer speeds have caught up with the data rates needed for wide-bandwidth pre-detection sampling, to the extent that computer clock rates are now within an order of magnitude of the observing frequencies used in centimetre-wavelength astronomy. These continuing advances permit commercially-available hardware to replace custom components in the construction of digital, phase-preserving baseband recorders. Such instruments are much more flexible than hardware detection systems, permitting variable filters and integration times, identification and excision of radio-frequency interference, and, if the data are stored on tape, multiple processing passes. In this paper we describe the Princeton Mark IV system, a baseband recorder developed primarily for pulsar astronomy and optimized for use with the Arecibo telescope; within the next few years we expect similar instruments to become valuable in many subfields of centimetre-wavelength astronomy, from radar ranging to spectroscopy.

## 2 DESIGN OF A BASEBAND RECORDER

One application of baseband recording is in high-precision timing and polarimetric observations of millisecond pulsars. Highly accurate pulsar timing has applications not only in the study of the pulsars themselves, but also in areas such as astrometry, time-keeping and experimental tests of cosmology and general relativity. An important obstacle to high timing precision is dispersion of the pulses during their propagation through the ionized interstellar medium. This phenomenon results in delays of lower-frequency radiation components relative to the higher frequencies, and across a typical observing bandwidth can amount to many (often hundreds or more) times the intrinsic pulse widths. The traditional pulsar timing and searching instrument has been an analogue filterbank system, in which the bandpass is subdivided into a number of channels, and the signal is detected in each channel and shifted by the predicted dispersion delay in order to align the pulse peak. This method inevitably leaves residual smearing within the channels, and the time resolution is limited to

the inverse of the channel bandwidth. If, instead, the data are sampled prior to detection, a frequency-domain “chirp” filter may be applied to remove completely the predicted effects of dispersion and align the pulse with no smearing. Timing precision is therefore greatly improved with this technique.

This “coherent dedispersion” method was pioneered more than two decades ago (Hankins & Rickett 1975), but until recently, the data storage and processing limitations discussed above resulted in mostly narrowband, hardware-based implementations, with special-purpose chips performing the convolution of the data stream with the chirp function (e.g., Stinebring et al. 1992). While large, multi-channel hardware dedispersion instruments are now in use (e.g., Backer et al. 1997), these systems record the data only after convolution and detection and hence do not permit reprocessing or interference excision. Baseband recording coupled with software dedispersion therefore offers a unique flexibility for the analysis of pulsar signals, and various different implementations have been presented in the literature (Jenet et al. 1997; Wietfeldt et al. 1998) and used for timing and single-pulse studies.

The design considerations for a pre-detection digital recorder include desired observing bandwidth, quantization resolution, recording medium, processing capability and cost and availability of components. In continuum applications, a wide bandwidth is needed for high signal-to-noise ratio; however the sampling and data rates scale linearly with bandwidth. To keep the data rate to a manageable level, it is therefore necessary to accept coarsely-sampled data; some techniques for optimizing signal quality in the case of 2-bit sampling will be discussed below. A further constraint on the feasible data rate is the speed of the recording medium, typically hard disk or magnetic tape. Wider observing bandwidths also require more computing power to process: the number of operations required may increase more rapidly than linearly if, for instance, Fourier Transforms are used in processing. The optimal balance between the different system components will depend on the goals determined for a particular instrument. For instance, the system described in Jenet et al. (1997) uses a custom VLSI chip to provide 2-bit sampling across 50 MHz of bandwidth, and records data to a high-speed tape recorder. Data processing is then carried out on supercomputers. Another implementation is the instrument described by Wietfeldt et al. (1998), in which a 16 MHz bandpass is quantized at 2 bits, and the data stream written to an adapted VLBI S2 recorder. Upon playback, the data may be analysed by a workstation or faster computer.

The Princeton Mark IV pulsar instrument was designed for use with the 8 MHz-wide 430 MHz line feed of the Arecibo radio telescope. The goal was to provide routinely us-

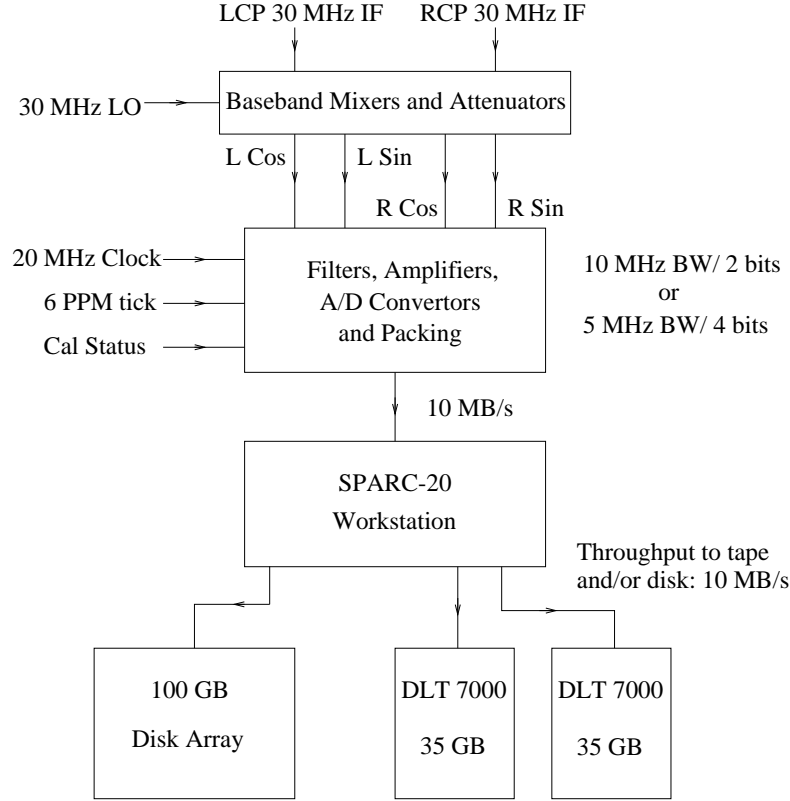


**Figure 1.** Block diagram of the Mark IV hardware.

able baseband sampling and recording across the full 8-MHz bandwidth using inexpensive hardware, commercially available recording media and an affordable dedicated processor. It provides somewhat greater flexibility than the systems discussed above, allowing 2-bit sampling across 10 MHz or 4-bit sampling across 5 MHz of bandwidth. Early prototypes of the system have been discussed in Shrauner et al. (1996) and Shrauner (1997). The final version, with a design based on the second prototype, is currently installed at the upgraded Arecibo Observatory.

### 3 MARK IV HARDWARE AND SOFTWARE IMPLEMENTATION

The Mark IV instrument accepts intermediate-frequency (IF) signals of bandwidth  $B$  (either 5 or 10 MHz) centred at 30 MHz. Adjustable attenuators regulate the signal strength, and the voltages are then mixed to baseband with quadrature local oscillators (LOs) at 30 MHz, producing, for each of two orthogonal polarizations, a real and an imaginary signal with passband 0 to  $B/2$ . These four signals are low-pass-filtered with a suppression in excess of

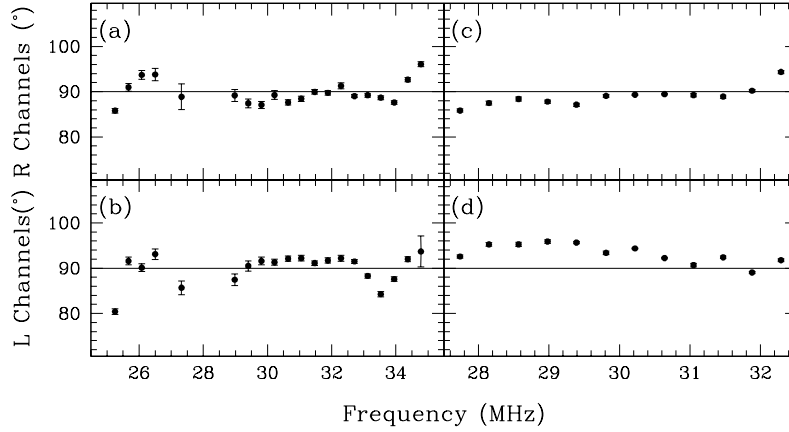


**Figure 2.** Mean phase differences at harmonics of 414 kHz between real and imaginary components of the left and right channels. Panels (a) and (b) display results for the 10 MHz bandpass; panels (c) and (d) for the 5 MHz bandpass. Some of the harmonics present in the 5 MHz bandpass do not appear in the 10 MHz plots because the 2-bit quantization was not sensitive to the lower signal strength.

60 dB at  $B/2$ , then 4-bit digitized at rate  $B$ , in accordance with the Nyquist theorem. Shift registers and multiplexers pack the samples such that all 4 bits are retained for the 5 MHz bandpass, while only the 2 most significant are kept for the 10 MHz bandpass. Thus the overall data rate is 10 MB/s regardless of bandwidth. This flow of data is piped through a DMA card into a SPARC-20 workstation and then onto a combination of hard disks and Digital Linear Tapes (DLTs) for off-line processing. The digitizer/packer board is clocked by a 20 MHz signal which is tied to the observatory time standard. The data timestamp is generated by a 10-second tick tied to the same external clock. The status of an injected noise signal may be monitored for later use in calibration. A block diagram of the system is shown in Figure 1.

In such a recording system hardware-related systematic errors may arise from the baseband mixers, from the low-pass filters, or from the amplifiers and attenuators in the signal path; care has been taken to minimize these errors. To verify the orthogonality of the baseband quadrature signals, a comb of harmonics of 414 kHz was used as an input signal. The data streams from the four input channels were separately Fourier-transformed and the phase differences between the real and imaginary components of the left and right channels were calculated at each harmonic. The results are plotted in Figure 2. The means cluster around  $90^\circ$ , as they should, with only slight variations across either bandpass. The absence

of some of the harmonics in the 10 MHz bandwidth plots (panels (a) and (b)) is due to the low intrinsic amplitude of the test signal at these frequencies.

The filters were selected for flat amplitude response with frequency; for other applications, constant response in phase may be more appropriate. Measurements indicate that the total phase rotation across the bandpass of one of the 5-MHz filters amounts to some 2.5 turns of phase. This extra shift could be incorporated into the chirp function; however, it is negligible relative to the thousands of turns of phase typically induced by dispersion. The amplitude response of the entire system is nearly flat as a function of frequency out to the knee of the filters.

### 3.1 Signal processing

The Mark IV system produces packed data at a rate of 10 MB/s, or 35 GB/hr. Analysis of this data stream in real time would require 8-10 Gflops. As an affordable alternative to a supercomputer, we use a 1.25 Gflop parallel processor optimized for Fast Fourier Transforms (FFTs), which form the core of the analysis. This machine, the SAM-350 from Texas Memory Systems, Inc., consists of 512 MB of fast memory, a DEC Alpha AX27 scalar processor, a parallel-processor board containing customized chips and an additional processor to handle communications. The fast memory may be accessed by the AX27, the parallel-processor board or a host workstation via an SBUS card.

Modeling the interstellar medium as a tenuous electron plasma permits the calculation of the “chirp” function used in the dedispersion analysis (Hankins & Rickett 1975):

$$H(f_0 + f_1) = \exp \left[ 2\pi i \frac{\text{DM}}{2.41 \times 10^{-10}} \frac{f_1^2}{f_0^2(f_0 + f_1)} \right], \quad (1)$$

where  $f_0$  is the central observing frequency in MHz,  $|f_1| \leq B/2$ , where  $B$  is the observing bandwidth, and the dispersion measure, given by  $\text{DM} = \int_0^d N_e dz$ , is the integrated electron density along the line of sight to the pulsar, measured in  $\text{pc cm}^{-3}$ . Coherent dedispersion is performed by transforming a segment of the baseband data to the Fourier domain, multiplying by the inverse of this chirp function and then transforming back to the time domain, with suitable overlap of successive data segments. In practice, the inverse FFT is taken in 2, 4 or 8 parts, splitting the bandpass into as many sub-bands. This permits the monitoring of potentially variable data quality (perhaps due to interference or scintillation) in different parts of the band, as well as the Faraday rotation of the linear polarization across the band.

Four cross-products are formed from the dedispersed data stream:  $|L|^2$ ,  $|R|^2$ ,  $\text{Re}(L^*R)$

and  $\text{Im}(L^*R)$ . These detected time series may be recorded directly and used in the analysis of single pulses. Usually, however, the data points for each sub-band and each cross-product are folded modulo the predicted pulse period and are summed into 10-second accumulated pulse profiles. The folded products are calibrated using the observed magnitude of a noise calibrator which is pulsed for one minute after a pulsar observation; the strength of the noise calibrator in Jy is known from comparisons with catalogue flux calibration sources. The Stokes parameters are readily calculated from the four recorded products; parallactic angle correction and polarimetry have been discussed elsewhere (Stairs, Thorsett & Camilo 1999).

Precise calculation of pulse times-of-arrival (TOAs) is essential to pulsar timing. The total-intensity folded profiles are cross-correlated with a standard template to measure the phase offset of the pulse within the profile (Taylor 1992). The offset is added to the time of the first sample of a pulse period near the middle of the data set to yield an effective pulse time-of-arrival.

### 3.2 Signal quality

Digital sampling is inherently a non-linear process: with less than an infinite number of bits, noise will inevitably be added to the signal. As the determination of precise times-of-arrival depends on accurate pulse profile shapes, preservation of the pulse shape is the primary concern in a coarsely-quantized pulsar observing system. The extreme case of 1-bit sampling, in which “on” and “off” values are assigned by comparing each sample to a running mean, yields the noisiest reproduced signal. Data rate considerations have motivated the choice of 2- and 4-bit sampling for the Mark IV system, an improvement on 1-bit sampling, but still coarse. This quantization will necessarily affect the observed pulse shapes and signal-to-noise ratios in statistically predictable ways.

Preserving the pulse profile in the case of 2-bit quantization requires some care. In this quantization process, the decision thresholds are  $-v_0$ , 0 and  $+v_0$  and the values assigned to the output levels are  $-n$ ,  $-1$ , 1 and  $+n$ , where  $n$  is not necessarily an integer. For a randomly fluctuating signal, Cooper (1970) finds a recoverable signal-to-noise ratio of 0.88 using  $n = 3$  and  $v_0$  equal to the root-mean-square voltage of the input signal,  $v_{\text{rms}}$ . However, in pulsar observations there is an additional complication: the signal is dedispersed after quantization. For the straightforward choice of  $v_0 = 1.0v_{\text{rms}}$  and  $n = 3$ , this process can result in the

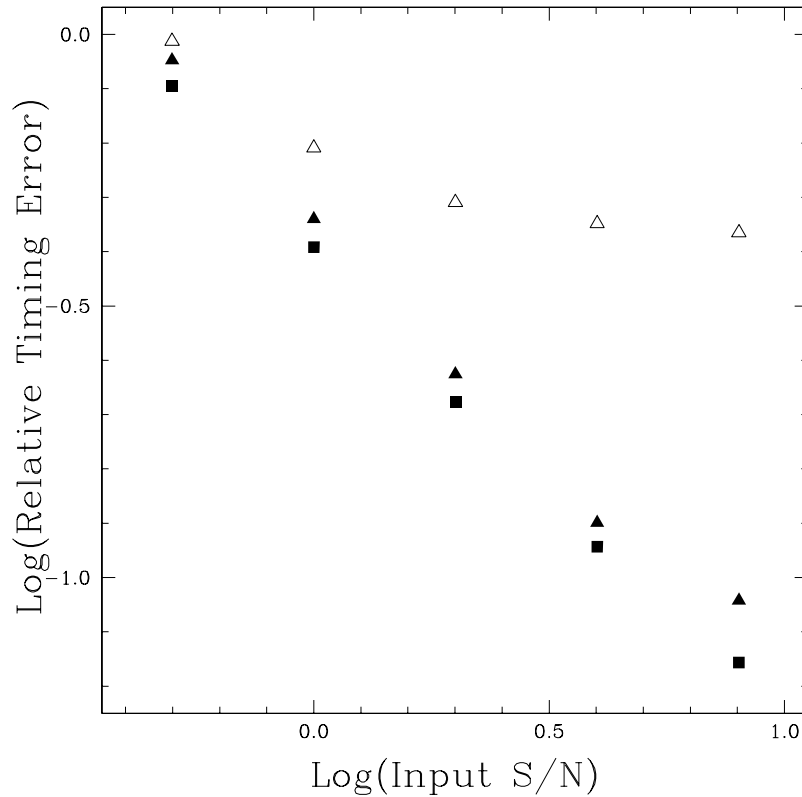


**Figure 3.** Root-mean-square uncertainties in the offset between the pulse recovered from the Monte Carlo quantization simulations and the original template for PSR B1534+12, as determined by the pulsar timing cross-correlation routine. The open triangles denote the results for 2-bit quantization,  $v_0 = 1.0v_{\text{rms}}$ ,  $n = 3$ , the solid triangles 2-bit quantization,  $v_0 = 1.4v_{\text{rms}}$ ,  $n = 4$  and the solid squares 4-bit quantization,  $v_0 = 0.59v_{\text{rms}}$  and evenly-spaced output levels. The latter two combinations show approximately linear behaviour with increasing input signal-to-noise ratio, indicating that the pulse profile is well-preserved under these quantization schemes.

appearance of dips to either side of the pulse when power is shifted to the aligned peak from the neighbouring regions of the profile (Jenet & Anderson 1998). This effect is most pronounced when the dispersion time across the observing bandwidth is comparable to the pulse width.

To find the quantization levels which minimize dips, we performed Monte Carlo simulations of observations with various quantization thresholds. The simulations used a high-resolution pulse profile of PSR B1534+12, dispersing, quantizing, dedispersing and accumulating 5000 of these pulses in each of 10 trials at each of several different initial signal-to-noise levels. The resulting profiles were then cross-correlated against the original profile, following the standard procedure used in pulsar timing. The uncertainty in the cross-correlation fit is therefore a measure of both the strength of the reproduced profile and its resemblance to the original. Figure 3 plots the root-mean-square cross-correlation uncertainties against



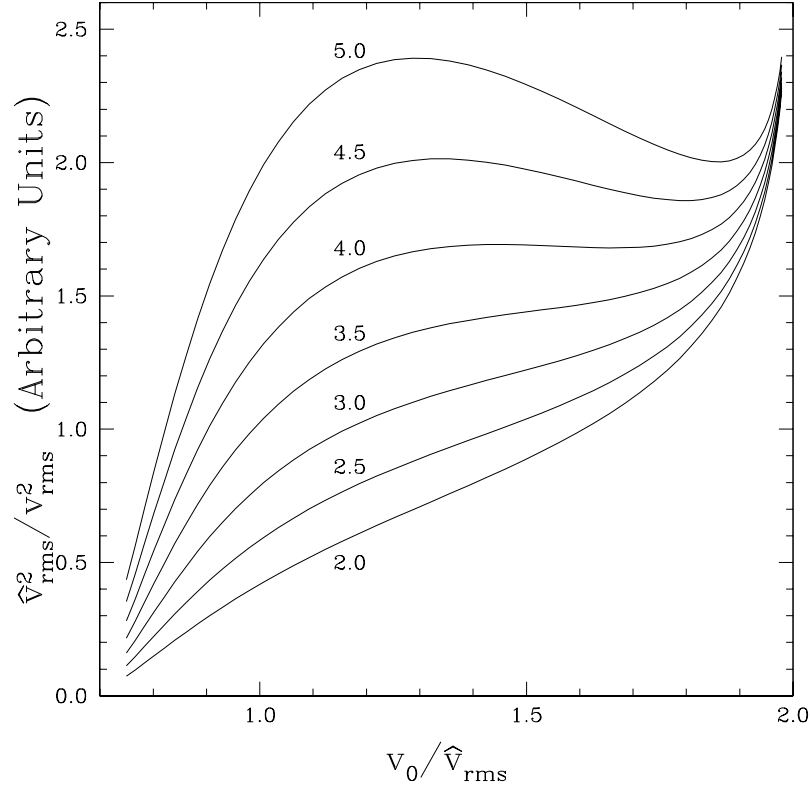


**Figure 4.** Ratio of quantized power to unquantized power (in arbitrary units) for different values of the quantization decision threshold  $v_0$  and outer level spacing  $n$ . Good linearity is achieved for  $n = 4.0$  in the domain around  $v_0 = 1.4\hat{v}_{\text{rms}}$ , where the response curve is nearly flat.

initial signal-to-noise ratio for 4-bit quantization with  $v_0 = 0.59v_{\text{rms}}$  and evenly-spaced output levels, for 2-bit quantization with  $v_0 = 1.40v_{\text{rms}}$  and  $n = 4$  and for 2-bit quantization with  $v_0 = 1.0v_{\text{rms}}$  and  $n = 3$ . It is apparent that the first two cases retain fairly good linearity across the range in question, where the strength of the individual pulses ranges from 0.5 of the system noise to 8 times the system noise, whereas the third case yields very poor reproductions of the original profile, particularly at higher signal-to-noise ratios. As the combination of  $v_0 = 1.40v_{\text{rms}}$  and  $n = 4$  for 2-bit quantization best eliminates dips and preserves the pulse shape, while making the final signal-to-noise ratio roughly 0.82 of the undispersed value, these parameters were adopted for all 2-bit observations.

In practice, the quantized  $\hat{v}_{\text{rms}}$  is estimated during data acquisition by calculating histograms of the incoming data using  $n = 3$ . The attenuation of the input voltage is then adjusted until the measured  $\hat{v}_{\text{rms}} = 0.71v_0$ . Thus the quantization threshold is set based on the quantized power rather than the unquantized power. Assuming a gaussian distribution of counts,  $\hat{v}_{\text{rms}}^2$  may be calculated analytically for any given  $v_0$  and  $n$ :

$$\hat{v}_{\text{rms}}^2 = \frac{1}{4} \left( n^2 + (1 - n^2) P \left( 0.5, 0.5 \left[ \frac{v_0}{v_{\text{rms}}} \right]^2 \right) \right), \quad (2)$$

where  $P(a, x)$  is the incomplete gamma function and the factor of  $1/4$  is an arbitrary normalization. Based on this calculation, the combination of  $n = 4$  and an input  $v_{\text{rms}}$  voltage such that  $v_0 \sim 1.4\hat{v}_{\text{rms}}$  yields very good power linearity. (Note that for  $n = 3$ ,  $v_0 = 1.4\hat{v}_{\text{rms}}$  implies  $v_0 \simeq 1.5v_{\text{rms}}$ .) The linearity as a function of  $v_0$  and  $n$  may be seen in Figure 4. The flat response for  $n = 4$  in the region around  $v_0 \sim 1.4\hat{v}_{\text{rms}}$  confirms the conclusions of the simulations.

Other procedures may still be necessary in order to recover the correct pulse shape. If there are very large power variations, for instance, the quantized power levels will often underestimate the true power and dips will result despite the  $n = 4$  correction. Jenet and Anderson (1998) overcome this problem in their 50-MHz baseband recorder by calculating the digitized  $\hat{v}_{\text{rms}}$  many times over the course of the predicted pulse period and dynamically adjusting  $n$  to preserve linearity. However, this method is not practical to compensate for very rapid fluctuations in system temperature during observations of the fastest pulsars. For example, the power in the pulsar signal may cause the telescope system temperature to fluctuate by a factor of 10 on time scale of  $1/1000$  of a period, perhaps  $2\mu\text{s}$ . With a sample rate of 10 MHz, this would allow only 20 samples per noise-level calculation, leading to estimation errors on  $v_{\text{rms}}$  on the order of  $20^{-1/2} \sim 20\%$ , too large to accurately adjust the output levels. Jenet and Anderson (1998) also discuss a correction for “scattered power” which becomes apparent in their band after dynamically setting  $n$ . With the fixed  $n = 4$  scheme, scattered power does not appear to be a problem. It is possible that the level-setting happens to be optimized to make the strength of residual dips and the scattered power exactly equal; however, as pulse-shape distortions are not evident, it appears that the existing scheme provides an adequate balance between efficient performance and high-quality signal reproduction.

#### 4 OBSERVATIONS WITH THE MARK IV INSTRUMENT

The Mark IV system and its prototypes have already been used for a variety of different observing purposes, such as studying single and giant pulses in PSR B1937+21 (Cognard et al. 1996), polarimetry of a large number of millisecond pulsars (Stairs, Thorsett & Camilo 1999), high-precision timing of millisecond pulsars, including the double-neutron-star binary

PSR B1534+12 (Stairs et al. 1998) and, using a software-synthesized filterbank, searches for the extremely fast pulsars that may exist in globular clusters. There have also been preliminary observations using the instrument as a backend for radar studies of asteroids; the instrument is clearly proving to be as flexible as hoped. Below we address the issue of greatest concern in pulsar timing: the time resolution obtainable with the new instrument relative to that obtained with the filterbank system it supersedes. We also discuss the short-term timing stability of the instrument and some interference-excision techniques developed during the course of the first observations with the completed system.

#### 4.1 Comparison with analogue filterbank

Pre-detection coherent dedispersion, as implemented in Mark IV, is expected to allow marked improvement in the precision of pulsar timing experiments relative to post-detection dedispersion systems, particularly in cases with substantial dispersion smearing within individual spectral channels. To investigate this, a series of test observations were made using the 305 m Arecibo telescope at 430 MHz. The Mark IV system collected data in parallel with the earlier Mark III system (Stinebring et al. 1992), which was commonly used for pulsar timing experiments before the recent Arecibo upgrade. For these observations, the Mark III system used a  $2 \times 32 \times 250$  kHz analogue filter bank to detect signals across an 8 MHz passband in two polarizations. The detected signals were low pass filtered with a time constant of  $100 \mu\text{s}$ , after which they were digitized and folded modulo the predicted topocentric pulse period.

##### 4.1.1 Expected precision of time of arrival measurements

The measurement of a pulse arrival time is made by fitting an observed pulse profile,  $p(t)$ , to a scaled, shifted high signal to noise ratio standard profile,  $s(t)$ :

$$p(t) = a + b s(t - \tau) + g(t) \quad (3)$$

where  $a$ ,  $b$  and  $\tau$  are constants, and  $g(t)$  represents random radiometer and background noise, and where  $0 < t < P$ , with  $P$  being the pulsar period. The quantity of greatest interest is the time shift  $\tau$  which, when added to the integration start time (along with a mid-scan correction), gives the pulse time of arrival.

The uncertainty in the arrival time is dominated by the uncertainty in  $\tau$ ,  $\sigma_\tau$ . In the limit where the pulsar is much weaker than the system noise, this uncertainty is (Downs & Reichley 1983):

$$\sigma_\tau = \frac{\sigma_n/b}{\left[\int_0^P (s'(t))^2 dt\right]^{1/2}}, \quad (4)$$

where  $s'(t)$  is the time derivative of the standard profile and  $\sigma_n$  is a measure of system noise. According to the radiometer equation,

$$\sigma_n \sim 1/(Bt)^{1/2} \quad (5)$$

where  $B$  is the bandwidth of detected radiation and  $t$  is the integration time. The ratio of timing precision of two observing systems, A and B, can therefore be written

$$\frac{\sigma_{\tau,A}}{\sigma_{\tau,B}} = \left( \beta \frac{B_B t_B}{B_A t_A} \right)^{1/2}, \quad (6)$$

where the shape factor  $\beta$  is defined by

$$\beta = \frac{\int (s'_B(t))^2 dt}{\int (s'_A(t))^2 dt}. \quad (7)$$

In the case of interest, system A is the Mark IV coherent dedispersion system and the profile  $s_A(t)$  is a close representation of the intrinsic pulse profile  $s_{\text{int}}(t)$  as emitted by the pulsar. System B is the Mark III post-detection dedispersion system. The observed pulse shape  $s_B(t)$  is the intrinsic pulse profile convolved with the effects of dispersion smearing and the detector time constant, calculated as follows.

The effect of dispersion smearing may be quantified by noting that the transmission function of the filters used by Mark III are well described by a Gaussian,

$$\phi(f_1) \sim \exp[-(f_1)^2/w^2] \quad (8)$$

where  $f_0$  is the centre frequency of the sub-band defined by the filter,  $f_1$  is a frequency within the filter sub-band, and with  $w = 125$  kHz is the filter half-width. To first order, the signal at frequency  $f = f_0 + f_1$  from a pulsar with dispersion measure DM is delayed by an amount  $t - t_0 = (1/\alpha) f_1$  relative to the centre of the sub-band, where the dispersion slope is

$$\alpha = \frac{1.205 \times 10^{-4} f_0^3}{\text{DM}} \frac{\text{pc cm}^{-3}}{\text{MHz}^2 \text{s}}. \quad (9)$$

Thus the intrinsic pulse profile is convolved with

$$\phi(\alpha t) = \exp[-(\alpha t/w)^2]. \quad (10)$$

Low pass filtering of the detected signal has the effect of further convolving the pulse profile with

$$\exp(-t/t_d), \quad (11)$$

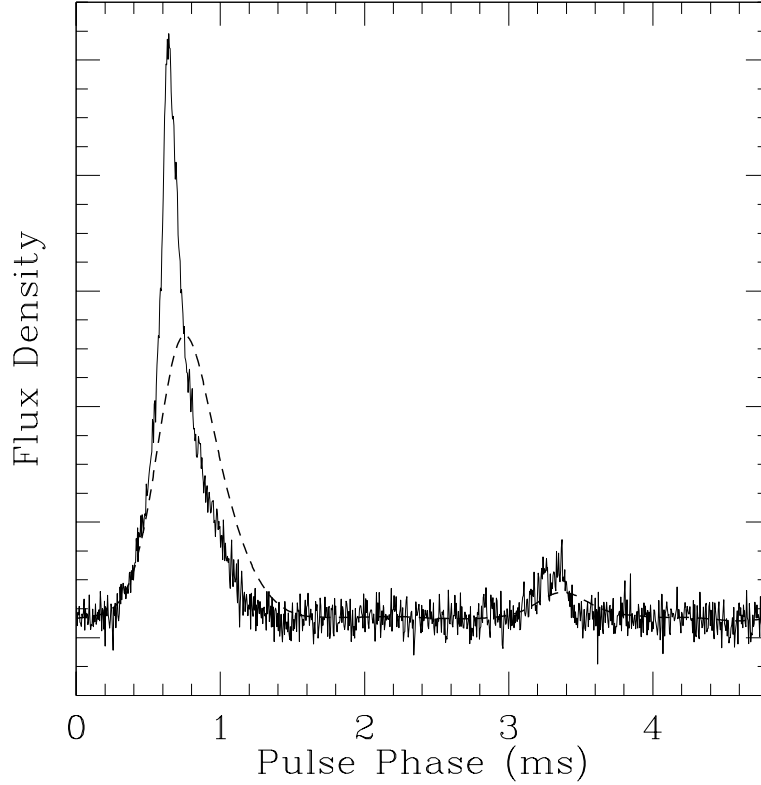


**Figure 5.** Pulse profile of PSR J2322+2057. *Solid line:* pulse profile at 430 MHz observed with Mark IV coherent dedispersion. *Dashed line:* The same profile, filtered by incoherent dedispersion as described in the text.

where  $t_d = 100 \mu\text{s}$  is the detector time constant.

The pulse profile expected to be observed by Mark III,  $s_B(t)$ , can be predicted by applying these convolutions to the intrinsic pulse profile as measured by Mark IV,  $s_A(t)$ . An example of a Mark IV profile shape and the same shape filtered by the Mark III system is shown in Figure 5. From such profiles, the shape factor  $\beta$  and expected improvement in timing precision,  $\sigma_{\tau,A}/\sigma_{\tau,B}$  can be derived. Values for the sources in our test observations are given in Table 1.

#### 4.1.2 Observations and results

For these observations, pulsars were selected for which dispersion smearing across a single channel was comparable to or larger than the intrinsic pulse width and the filter bank time constant. Sources were observed simultaneously with the Mark III and Mark IV systems, typically for 29 or 58 minutes on a given day. Mark III covered a bandwidth of  $B_A = 8 \text{ MHz}$  (except for one observation; see Table 1). Mark IV covered a bandwidth of  $B_B = 5 \text{ MHz}$

**Table 1.** Comparison of Mark III and Mark IV timing residuals

Pulsar Name	P (ms)	DM (pc cm <sup>-3</sup> )	Date (MJD)	$t_B$ (s)	$\beta$	Predicted $\sigma_{\tau,B}/\sigma_{\tau,A}$	$\sigma_{\tau,A}$ ( $\mu$ s)	Observed $\sigma_{\tau,B}$ ( $\mu$ s)	$\sigma_{\tau,B}/\sigma_{\tau,A}$
J0621+1002	28.8	36.6	51138	123	0.56	0.56	5.0	2.8	0.55
J0751+1807	3.5	30.3	51138	183	0.21	0.26	9.0	3.2	0.36
J1022+1001	16.5	10.2	51138	123	0.62	0.62	3.2	1.5	0.48
J2019+2425	3.9	17.2	50995	130	0.30	0.31	27.3	3.5	0.13
J2019+2425	3.9	17.2	51138	130	0.30	0.31	19.1	6.8	0.37
J2322+2057	4.8	13.4	51138*	183	0.33	0.38	4.5	1.3	0.30
J2322+2057	4.8	13.4	51139	23	0.33	0.15	33.4	3.8	0.11

Note. – Mark IV: B=5 MHz, t=190 s always; Mark III: B=8 MHz except observation noted by \*, for which B=6.75 MHz.

with 4-bit sampling. Integration time for Mark III varied; see Table 1. Integration time for Mark IV was fixed at  $t_A = 190$  s. Combining these bandwidths and integration times resulted in the predicted ratio of timing residuals (see Table 1).

Data from each observing system was reduced by calculating pulse arrival times and fitting to a pulsar timing model with the standard TEMPO (<http://pulsar.princeton.edu/tempo>) program. The root-mean-square values of the residuals from these fits are tabulated as  $\sigma_{\tau,A}$  and  $\sigma_{\tau,B}$ .

In most cases Mark IV improved the timing precision as much as, or more than, expected. There are several possible sources of improvement beyond the predicted values. (1) Mark IV has better interference removal, since individual points in the time series are examined, as described in §4.3 below. (2) Variations in pulsar flux density within individual spectral channels of the Mark III system cause non-uniform dispersion smearing, resulting in biased arrival times. (3) Small errors in the calibration of the analogue filter bank could lead to errors of several microseconds.

## 4.2 Short-term timing stability

If there are no systematic effects in a set of timing data, the root-mean-square deviation of the times-of-arrival from the predicted model should decrease as  $t_{\text{int}}^{-1/2}$ , where  $t_{\text{int}}$  is the integration time for the TOAs. To test whether this holds true for Mark IV data, the millisecond pulsars PSRs B1937+21 and J1713+0747 were observed for 30 minutes with 10 MHz bandwidth at the Arecibo Observatory. TOAs were then calculated for integration times ranging from 1 s to 640 s and fitted to the pulsar timing model using the TEMPO program. The rms postfit residuals were calculated for each integration length; they are displayed as a function of  $t_{\text{int}}$  in Figure 6. For PSR J1713+0747, the residuals closely follow

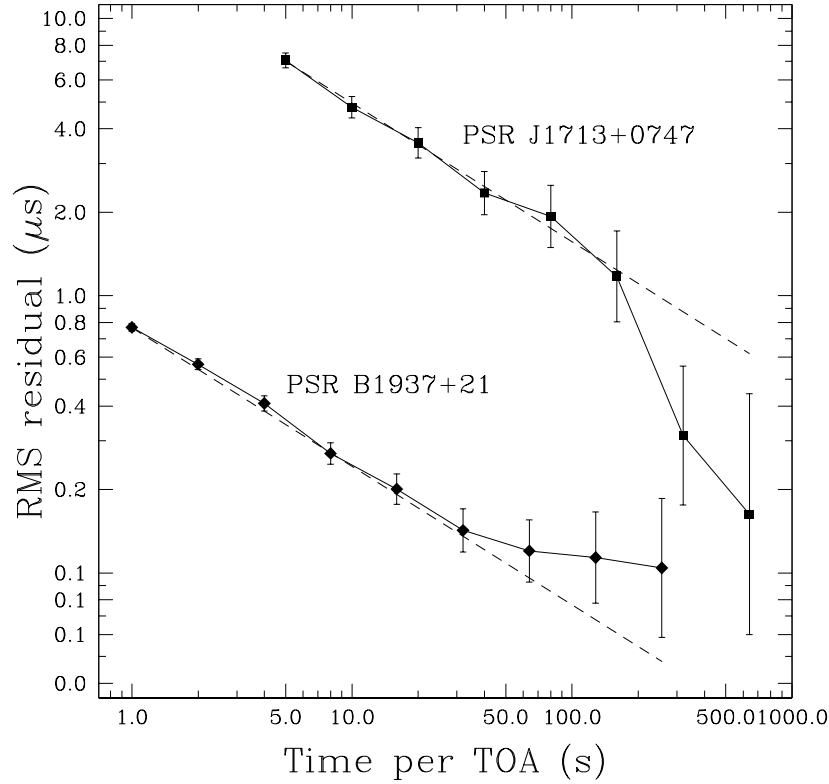


**Figure 6.** Root-mean-square postfit timing residuals for the millisecond pulsars PSRs B1937+21 and J1713+0747, as functions of the length of time  $t$  used for the time-of-arrival integrations. The dashed lines indicate slopes corresponding to  $t^{-1/2}$ . See the text for a discussion of the departures from this predicted slope.

the expected slope of  $t_{\text{int}}^{-1/2}$ ; the apparent drop for large integration times can be explained by small-number statistics. For PSR B1937+21, the rms residuals follow the expected slope until leveling off at a deviation of approximately 100 ns, indicating that systematic effects prevent greater timing precision.

It is likely that the systematic effects limiting the timing precision of PSR B1937+21 are not due to the Mark IV instrument but rather to the variability of the pulses reaching the Earth. Although PSR B1937+21, with a spin period of 1.56 ms, is the fastest pulsar known, and is indeed one of the most stable (Kaspi, Taylor & Ryba 1994), its emission is subject to significant scattering by the interstellar medium. This process has the effect of convolving the pulse profile with a variable exponential tail, resulting in slightly changed observed profiles and hence an unavoidable uncertainty in the TOA calculation. The magnitude of this uncertainty can be estimated by considering the pulsar scintillation due to diffraction in the interstellar medium. The size of the scintillation features can be described by the

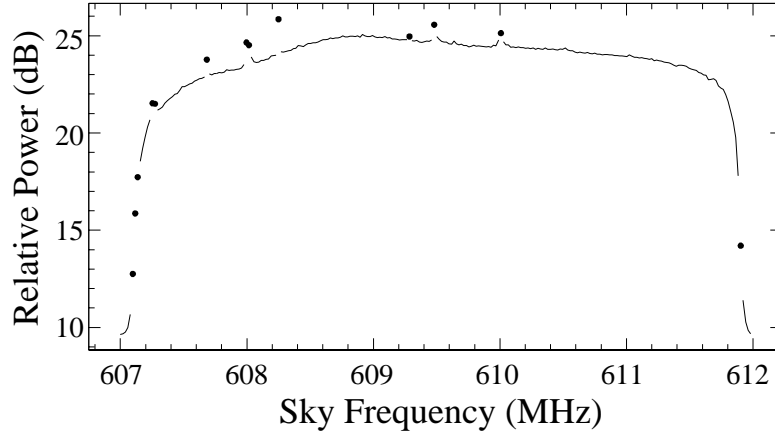


**Figure 7.** An example of narrowband interference excision. The connected lines are the acceptable parts of the spectrum; the points are those frequency bins that have been masked by the interference-hunting algorithm.

decorrelation bandwidth,  $\Delta\nu$ , and scintillation timescale,  $\Delta t$ , for a given observing frequency. At 1400 MHz, these parameters for PSR B1937+21 have been found to be roughly  $\Delta\nu = 0.83$  MHz and  $\Delta t = 400$  s (Rawley, Taylor & Davis 1988), leading to a scattering timescale of  $\tau_s = 1/(2\pi\Delta\nu) = 190$  ns. The portion of the timing uncertainties due to scattering-induced profile changes should be roughly equal to  $\sigma_{\text{TOA}} = \tau_s \sqrt{\Delta\nu/B}$  (Cordes et al. 1990), where  $B$  is the observing bandwidth, yielding a minimum uncertainty of 55 ns for the 10 MHz bandpass of the Mark IV observations. While this is somewhat smaller than the observed lower bound on the timing uncertainties, the order of magnitude is correct, and indicates that the largest part of the remaining residuals is due to scattering-induced variations of the pulse profile rather than to instrumental systematics. Furthermore, the timing analysis shows that roughly halfway through the observation, the profile strength weakened considerably due to scintillation for about 10 minutes, increasing timing uncertainties for this period by roughly a factor of two. Variable data quality will also prevent the residuals from integrating down as predicted. Though it is possible that there may be some instrumental effects at the 50 ns level, deriving, for instance, from the 20 MHz clock signal, it appears from these observations that the overall timing properties of the Mark IV instrument are satisfactory.



### 4.3 Interference excision

An increasingly important problem facing radio astronomy is that of radio frequency interference. Communications satellites, television stations and other transmitters render even the protected astronomy bands in the radio spectrum vulnerable to noise. Though negotiations may bring about stronger protections, it is also useful to develop data-acquisition instruments which are capable of mitigating its effects. Baseband recording systems permit interference to be eliminated in software; the techniques discussed here could easily be adapted for applications beyond pulsar observations.

The Mark IV processing includes, optionally, two types of interference excision: narrowband and broadband. For narrowband excision, a short (typically 256-point) power spectrum is computed for every tenth FFT segment. A simple algorithm searches through the spectrum, calculating 5-point medians about every frequency bin and flagging each point which differs from its corresponding median by more than 4%, or which differs from both its nearest neighbours by more than 50%. Subsequently, points with both nearest neighbours or at least three of four nearest neighbours flagged are also flagged. A mask is produced which is used to zero the contaminated frequencies in the next set of data segments. On average, 5 to 10% of frequency points are zeroed in this fashion, with no apparent effect on the resulting pulse shape. Figure 7 shows a typical spectrum and resulting mask.

Broadband noise is eliminated by searching through the packed data samples for power spikes greater than 30 times the root-mean-square noise above the median. If such spikes are found, the samples in question are set to zero. This algorithm is extremely effective at eliminating broadband noise, again with no apparent effect on the pulse profile shape. “Before” and “after” grayscale plots of an interference-contaminated observation are shown in Figure 8. The benefits of interference excision may be easily deduced from this figure: in some of the 10-second integrations in the first analysis, the pulsar is drowned out by the interference and does not appear at all, whereas in the second analysis it is always present. The baseline of the overall pulse profile is also much improved. This technique not only improves the signal-to-noise ratio, but also eliminates a large source of systematic error in the time-of-arrival fitting.

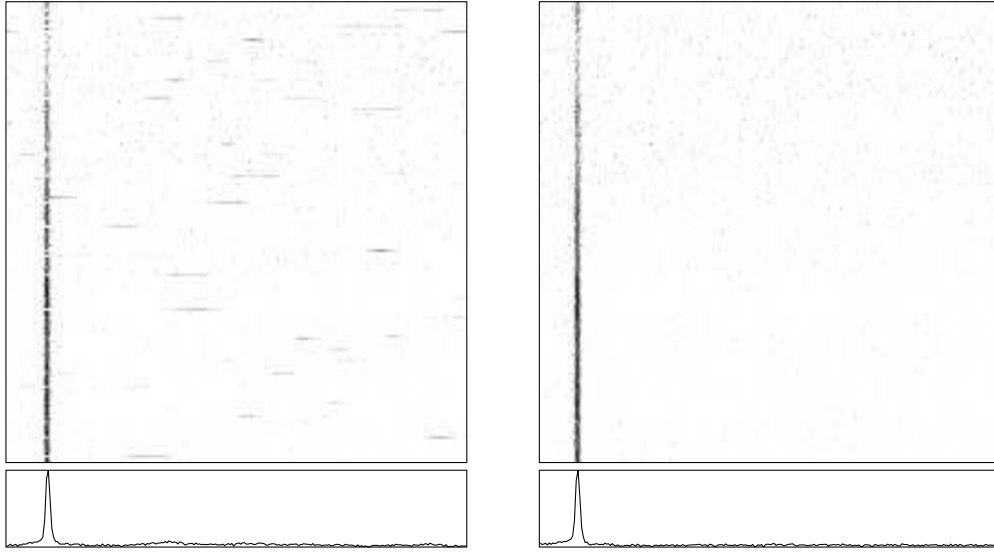


**Figure 8.** An example of broadband interference excision. The left panel shows a grayscale plot of a contaminated 29-minute 610 MHz observation of PSR B1534+12 taken with the 76 m telescope at Jodrell Bank, U.K. Each horizontal line represents ten seconds of data, and a cumulative pulse profile is displayed at the bottom. The broadband interference spikes have been “dedispersed” by roughly 6% of the pulse period, yielding the smeared-out bumps seen in the left-hand panel. The right panel presents the same observation, but with these broadband power spikes eliminated during processing.

## 5 CONCLUSION

The Mark IV system provides an example of a 10 MHz baseband recording system designed for use in pulsar observations. It meets and exceeds the predicted improvements in timing precision over earlier filterbank systems, and the analysis code contains features allowing optimal profile-shape recovery for 2-bit quantization and the excision of narrowband and broadband interference. These improvements could easily be generalized for application to other types of observations.

Future designs of pre-detection digital recorders will likely take advantage of the availability of more powerful computers and faster recording media to produce instruments with wider bandwidths. The performance-to-cost ratio of computers tends to increase exponentially, doubling every 18 months. Disk storage also becomes faster and less expensive with time, while the cost of magnetic tapes tends to remain more stable, thus the temptation is to migrate toward wide-bandwidth systems with only disk storage. Naturally, for an instrument in which the data are processed directly from disk and overwritten by subsequent observations, the reprocessing capability provided by the more expensive and slower tape storage

will be lost. However, there are justifiable reasons for moving to such a scheme. At frequencies above 1 GHz, for instance, pulsar signals are often so weak that more than 10 MHz observing bandwidth is required to obtain usable signal-to-noise ratios. Further, although the precision of measurements from strong, distant pulsars will be limited by scattering, as discussed in §4.2, improved signal-to-noise ratio is useful for nearly all other observations. Finally, the inherent flexibility of baseband recording systems should encourage the development of instruments which can be used for a multitude of different types of centimetre-wavelength observations.

## ACKNOWLEDGEMENTS

We thank Hal Taylor, Jay Shrauner and Phil Perillat for work in designing the Mark IV prototypes, Bob Wixted for helpful discussions, Stan Chidzik for laying out and assembling the circuit boards, Mark Krumholz, Christopher Scaffidi and Donald Priour for hardware work and Walter Briskin for SAM-350 software testing. The Arecibo Observatory, a facility of the National Astronomy and Ionosphere Center, is operated by Cornell University under a cooperative agreement with the U. S. National Science Foundation. I. H. S. received support from an NSERC 1967 fellowship. S. E. T. is an Alfred P. Sloan Research Fellow. This work was supported by the NSF and the Seaver Institute.

## REFERENCES

- Backer D. C., Dexter M. R., Zepka A., Ng D., Werthimer D. J., Ray P. S., Foster R. S., 1997, *Publ. Astr. Soc. Pacific*, 109, 61
- Cognard I., Shrauner J. A., Taylor J. H., Thorsett S. E., 1996, *Astrophys. J. Lett.*, 457, L81
- Cooper B. F. C., 1970, *Aust. J. Phys.*, 23, 521
- Cordes J. M., Wolszczan A., Dewey R. J., Blaskiewicz M., Stinebring D. R., 1990, *Astrophys. J.*, 349, 245
- Downs G. S., Reichley P. E., 1983, *Astrophys. J. Supp. Series*, 53, 169
- Hankins T. H., Rickett B. J., 1975, *Meth. Comp. Phys.*, 14, 55
- Jenet F. A., Anderson S. B., 1998, *Publ. Astr. Soc. Pacific*, 110, 1467
- Jenet F. A., Cook W. R., Prince T. A., Unwin S. C., 1997, *Publ. Astr. Soc. Pacific*, 109, 707
- Kaspi V. M., Taylor J. H., Ryba M., 1994, *Astrophys. J.*, 428, 713
- Rawley L. A., Taylor J. H., Davis M. M., 1988, *Astrophys. J.*, 326, 947
- Shrauner J. A., 1997, PhD thesis, Princeton University
- Shrauner J. A., Stairs I. H., Dewey R. J., Krumholz M., Taylor H. E., Taylor J. H., Thorsett S. E., 1996, in Johnston S., Walker M. A., Bailes M., eds, *Pulsars: Problems and Progress*, IAU Colloquium 160. Astronomical Society of the Pacific, San Francisco, p. 23
- Stairs I. H., Arzoumanian Z., Camilo F., Lyne A. G., Nice D. J., Taylor J. H., Thorsett S. E., Wolszczan A., 1998, *Astrophys. J.*, 505, 352
- Stairs I. H., Thorsett S. E., Camilo F., 1999, *Astrophys. J. Supp. Series*, 123, 627

- Stinebring D. R., Kaspi V. M., Nice D. J., Ryba M. F., Taylor J. H., Thorsett S. E., Hankins T. H., 1992, *Rev. Sci. Instrum.*, 63, 3551
- Taylor J. H., 1992, *Phil. Trans. Roy. Soc. A*, 341, 117
- Wietfeldt R., Van Straten W., Del Rizzo D., Bartel N., Cannon W., Novikov A., 1998, *Astr. Astrophys. Suppl. Ser.*, 131, 549